Design of smart metamaterials for vibration control: extension of Bloch approach to handle finite system boundary conditions

Kévin Billon, Morvan Ouisse, Manuel Collet, Emeline Sadoulet

Design of smart metamaterials for vibration control: extension of Bloch approach to handle finite system boundary conditions

K. Billon[a], M. Ouisse[a], M. Collet[b], and E. Sadoulet-Reboul[a]

[a]Univ. Bourgogne Franche-Comté FEMTO-ST Institute CNRS/UFC/ENSMM/UTBM, Department of Applied Mechanics, 24 chemin de l'Epitaphe, 25000 Besançon, France
[b]Laboratory of Tribology and Systems Dynamics (LTDS), École Centrale de Lyon, 36 avenue Guy de Collongue, 69134 Ecully, France

ABSTRACT

The design of smart metamaterials for vibration control is usually based on the use of Bloch theorem which considers a single cell with adequate boundary conditions. These boundary conditions correspond to the infinite repetition of the unit cell in 1D, 2D or 3D. Complex geometries and composite systems can then be designed using this approach with finite elements. The control of the elastic waves can be performed by combining Bragg's (wave interferences), resonant's (resonance of a component embedded in the unit cell), damping and/or active control. The energy can then be reflected, transmitted, damped, focused or confined in a specific zone of the structure. However, the practical realization of real-life 2D or 3D finite systems may lead to some situations where energy transfers are not in accordance with those predicted by the infinite system considered in the design, because of reflections on the boundary conditions of the finite structure. The behavior of the system may be simulated by full system modelling, but this is time consuming and may lead to huge calculation costs. In this paper, we propose an extension of the Bloch approach to handle finite system boundary conditions in order to be able to identify situations in which energy transfer may arise because of reflections on the border of the elastic domain. Calculations are performed on 2 cells with adequate boundary conditions. The methodology is described and validated using full finite model and experimental tests on a 2D metamaterial structure.

Keywords: Periodic structures, Metamaterial, Dispersion, Dissipation, Vibroacoutic.

1. INTRODUCTION

A periodic medium is a material or a structural system that exhibits spatial periodicity.[1] The study of periodic structures has a long history in the field of vibrations and acoustics.[2] This topic has interested researchers over the years, and a growing activity on this field is observed on the last years, with the objective of designing structures exhibiting properties that conventional ones cannot possess.[3–5] The methods currently used are most of the time based on those derived from wave propagation in crystals,[6] where almost no dissipation occurs. The classical Floquet-Bloch approach[7,8] is a method commonly used for the study of periodic structures. The material constitutive law is linear, elastic and isotropic. The periodicity is defined on the borders of the domain $u_R = e^{-jk_x r}u_L$ and $v_R = e^{-jk_y r}v_L$ where u_R (resp. v_R) is the displacement on the right border and u_L (resp. v_L) is the displacement on the left border in x (resp. y) axis, k_x and k_y are respectively the wavenumbers in the x and y directions[9,10] for details.

Further author information: (Send correspondence to Morvan Ouisse)
E-mail: morvan.ouisse@femto-st.fr, Telephone: +33 3 81 66 60 00

2. METAMATERIAL DESIGN

The metamaterial consists in an infinite periodic bidirectional waveguide.[11–13] It is a 1 mm thick plate with periodic cylindrical pillars. In order to design a two-state phononic crystal, a polymeric base is included in the pillar (figure 1). The base plate is made of isotropic Aluminium 6063-T83 ($\nu = 0,33, E = 69\ GPa$ and $\rho = 2700\ kg/m^3$). Pillars are made of combination between a highly dissipative polymer tBA/PEGDMA ($\nu_{poly} = 0,37, E_{poly}$, defined in the following and $\rho_{poly} = 1004[kg/m^3]$)[14] and Aluminum 6063-T83.

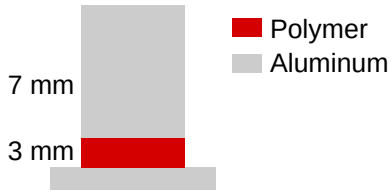

Figure 1. Metamaterial with 3 mm height polymeric interface between base and 7 mm height aluminum cylinder.

The polymer thickness has been chosen in order to open a resonant bandgap under the bragg bandgap frequency. According to the manufacturing process, the maximum thickness obtained after the UV photopolymerization is 3 mm. The natural frequency is around 40 kHz in this case. The eigenshape of the corresponding mode is shown in figure 2.

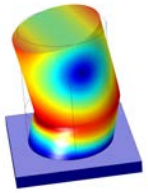

Figure 2. Eigenshape at 40 kHz.

A suitable model is required for the description of the frequency-dependent behaviour of the polymer. In the harmonic regime, the Young's modulus of the polymer is complex, dependent on frequency and temperature,

$$E^*_{poly}(\omega) = E' + jE'' = E' \times (1 + j \times tan(\delta)), \tag{1}$$

where $tan(\delta) = E''/E'$ is the loss factor, E' is the storage modulus and E'' is the loss modulus. In this work, a fractional derivative Zener[15] model is used. This material exhibits a strong temperature dependency but in this case, at ambient temperature 25°C, E^*_{poly} is constant ($E' = 2.21\ GPa$ and $tan(\delta) \approx 0$).

3. DYNAMICAL PROPERTIES

3.1 Dispersion analysis

The "Shifted-cell operator" technique is used to obtain dispersion curves along the $\Gamma - X$ direction in.[9] Damping is included in the analysis according to complex polymer Young's modulus using fractional derivative Zener model and aluminum loss factor equal to 0.5%.

Figure 3a shows dispersion curves along the $\Gamma - X$ direction obtained with the "Shifted-cell operator" method using branch tracking. The associated group velocity is plotted figure 3b. The bandgap is visible around the selected frequency (40 kHz) linked to the design of the resonator.

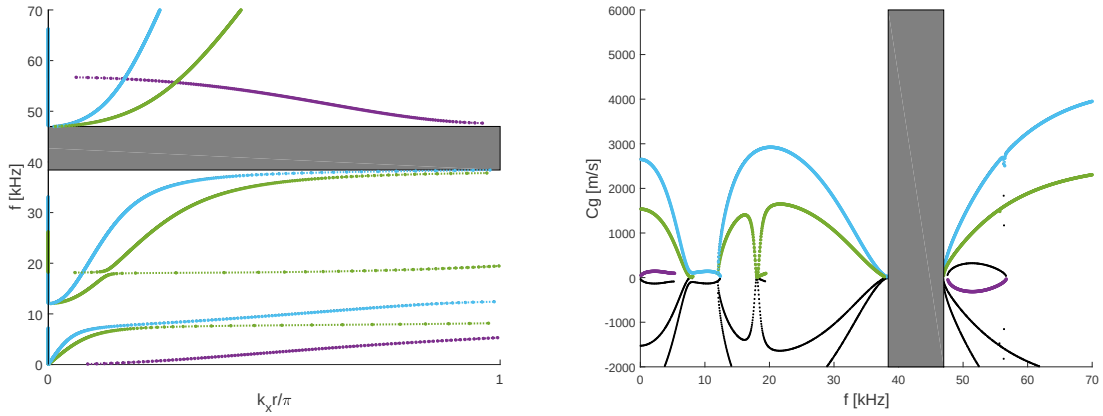

(a) (b)

Figure 3. a) Dispersion curves along the $\Gamma - X$ direction obtained with the "Shifted-cell operator" method. b) Group velocity associated to dispersion curves. Grey shapes represent bandgaps.

3.2 Finite structure

The main goal of this part is to validate in a finite structure the phenomenon observed on an infinite structure. A finite element model is presented. This is followed by an experimental validation. The metamaterial ($21 \times 7 \times 0.1\ cm^3$) includes an interface composed by 7×7 unit cells (figure 4).

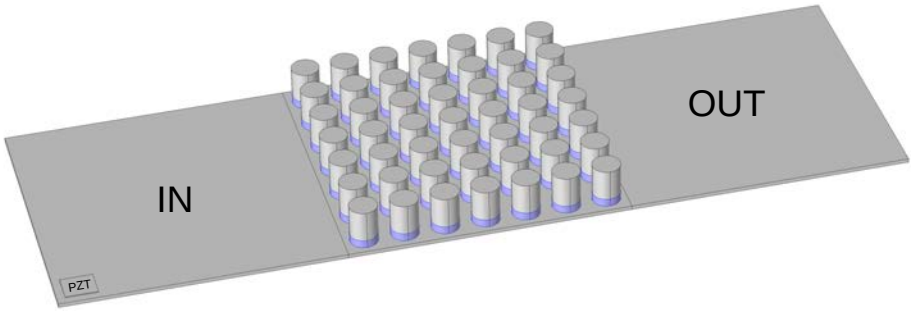

Figure 4. Finite structure with an interface composed by 7×7 unit cells distributed. Piezoelectric patch (PZT) for excitation in the bottom left corner.

A piezoelectric patch with harmonic voltage ($|U| = 100\ V$) is included in the model in order to be close to the experimental set up and cover all the frequency range from 0 to 50 kHz. Figure 5 shows numerical frequency responses ($|Vz|^2/U^2$) obtained with the finite elements code. Squared velocity amplitudes $|Vz|^2$ are averaged for the input plate (IN) and the output plate (OUT) and U is the voltage generated across piezoelectric patch. Blue and red curves are numerical frequency response for the input plate (IN) and the output plate (OUT). The grey shape represents the bandgap predicted by the dispersion analysis.

An output attenuation ($\Delta f = 3.1\ kHz$) around 40 kHz is observed smaller than the frequency range predicted by bandgap ($\Delta f = 8.9\ kHz$).

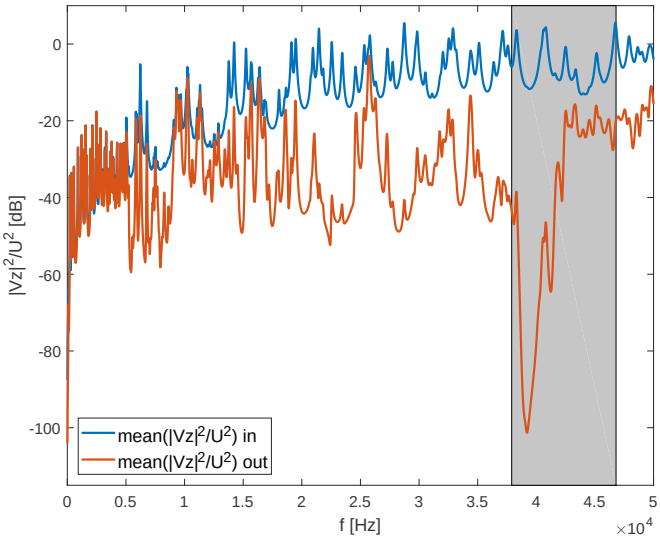

Figure 5. Numerical frequency responses. Average squared velocity amplitude $|Vz|^2$ for the input plate (IN) and the output plate (OUT) respectively in blue and red. The grey shape represents the bandgap predicted by the dispersion analysis.

Figure 6a represents numerical frequency responses focus on the frequency range of the bandgap. 4 points are selected in the frequency response, 2 outside (34.4 kHz, 50.0 kHz) and 2 inside (39.2 kHz, 43.3 kHz) the predicted bandgap. Corresponding operational deflections are visible on figures 6b, 6c, 6d and 6e.

Energy can propagate through the lattice at 34.4 kHz (figure 6b) and 50.0 kHz (figure 6e), these 2 frequencies are outside the predicted bandgap. At 39.2 kHz, inside the bandgap, the attenuation is widely visible, all the energy is confined in the input plate (IN).

At 43.3 kHz, the lattice is not efficient despite the fact that the frequency of interest is located inside the predicted bandgap. After shapes analysis, the vibration level is near to zero in the middle of the lattice but the energy propagates along the edges of the periodic lattice. Energy transmission occurs along the edges, and the dispersion analysis can not predict this effect.

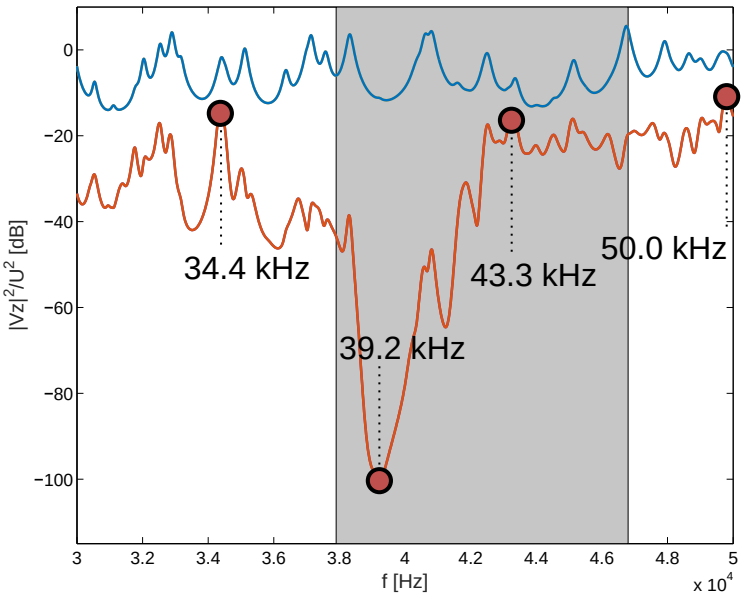

(a) num - FRF

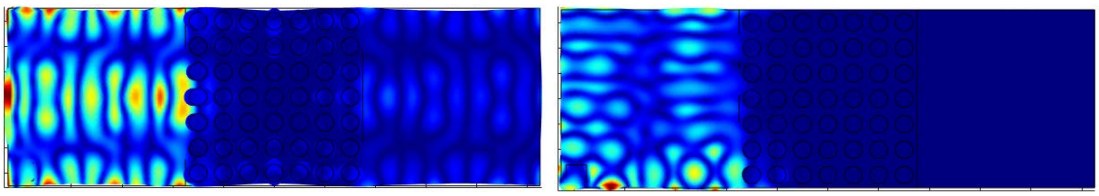

(b) num - 34.4 kHz

(c) num - 39.2 kHz

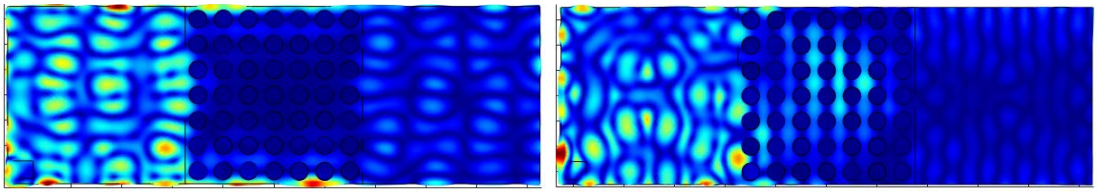

(d) num - 43.3 kHz

(e) num - 50.0 kHz

Figure 6. a) Zoom on numerical frequency responses. Average squared velocity amplitude $|Vz|^2$ for the input plate (IN) and the output plate (OUT) respectively in blue and red. The grey shape represents the bandgap predicted by the dispersion analysis. Several points are selected with corresponding deformed shapes b) at 34.4 kHz, c) 39.2 kHz, d) 43.3 kHz and e) 50.0 kHz.

3.3 Experimental validation

The metamaterial is made of metal and polymer. Polymer parts are realised by laser cutting and metallic part by classical mechanical processing (figure 7). The metamaterial is assembled in two steps by bonding parts together. Polymer cylinders are sticked on the support plate. After drying and load process, at ambient temperature during 24 hours, aluminum cylinders are sticked on polymer cylinders. Piezoelectric patch provides harmonic excitation up to 50 kHz.

The metamaterial is suspended to reproduce free boundary condition as shown in figure 8.

The white noise generator provides random harmonic voltage (5 V) between 500Hz and 50kHz, this signal is amplified 20 times by the piezoelectric amplifier. A 3D vibrometer is used to measure the velocity and frequency

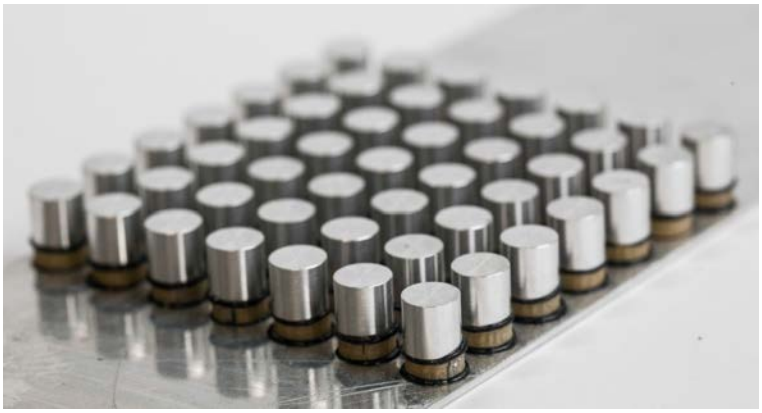

Figure 7. Metamaterial after several manufacturing steps.

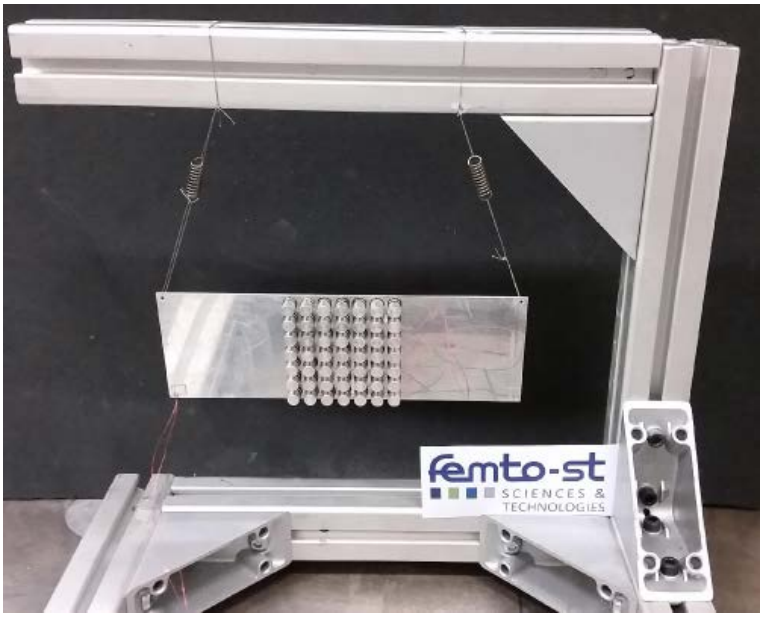

Figure 8. Metamaterial in suspended configuration.

responses are calculated with $H1$ estimator.

The experimental analysis is focused on the 4 frequency points pointed out in the numerical part. Figures 9 show experimental deformed shapes at 33.4 kHz, 38.2 kHz, 42.2 kHz and 50.0 kHz corresponding to numerical deformed shapes (Figure 6). Shapes are similar between numerical and experimental results. In particular, it can clearly be observed in figure 9c that the energy is transported along the borders. This observation being experimentally validated, the next section aims at proposing a new methodology to identify such configurations using cell-based computation.

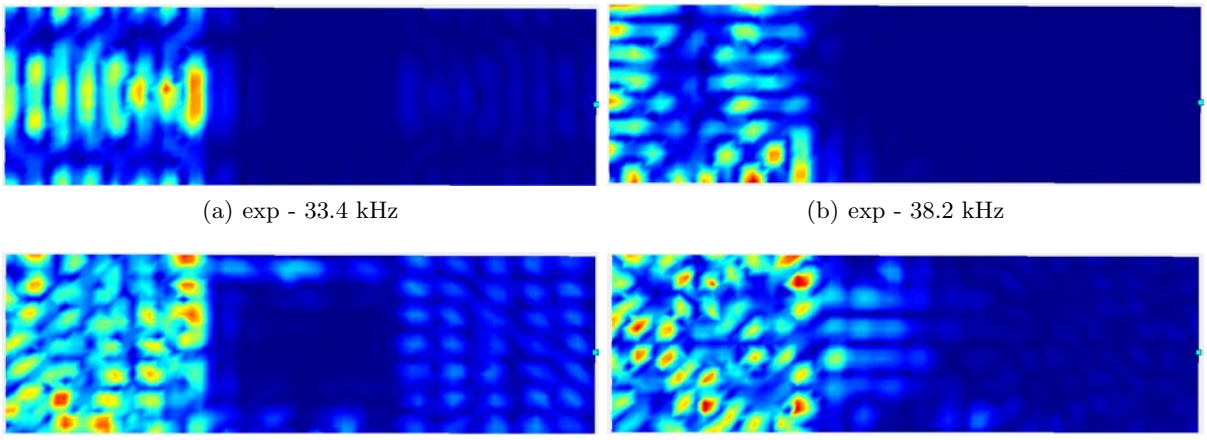

(a) exp - 33.4 kHz (b) exp - 38.2 kHz

(c) exp - 42.2 kHz (d) exp - 50.0 kHz

Figure 9. Experimental deformed shapes a) at 33.4 kHz, b) 38.2 kHz, c) 42.2 kHz and d) 50.0 kHz corresponding to numerical deformed shapes (Figures 6).

4. EXTENSION OF BLOCH APPROACH

Two connected cells are considered in the analysis (figure 10). Bondary conditions are as follow:

- in the y direction, classical Floquet-Bloch conditions are used, namely $v_R = e^{-jk_y r} v_L$ where v_R is the displacement on the right border and v_L is the displacement on the left border in y axis,
- the x direction, displacement on the left border is linked to the displacement of the connected line $u_R = e^{+jk_x r} u_L$, while the right border uses the effective boundary conditions (free end in our case).

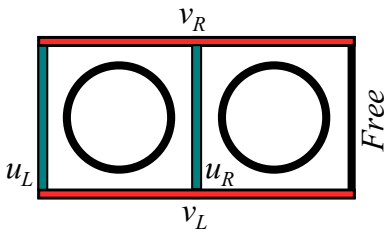

Figure 10. Boundary conditions of the 2 cells system.

11a shows dispersion curves along Brillouin zone obtained with the "Shifted-cell operator" method for the 1 cell and 2 cells system. The blue curve corresponds to the 1 cell dispersion curve (figure 3a). The dispersion for the 2 cells system is plotted in red, a branch appears in the bandgap and the corresponding deformed shape is visible in the figure 11b. The shape is the same as the eigenshape but energy can propagate in the y direction along the free border.

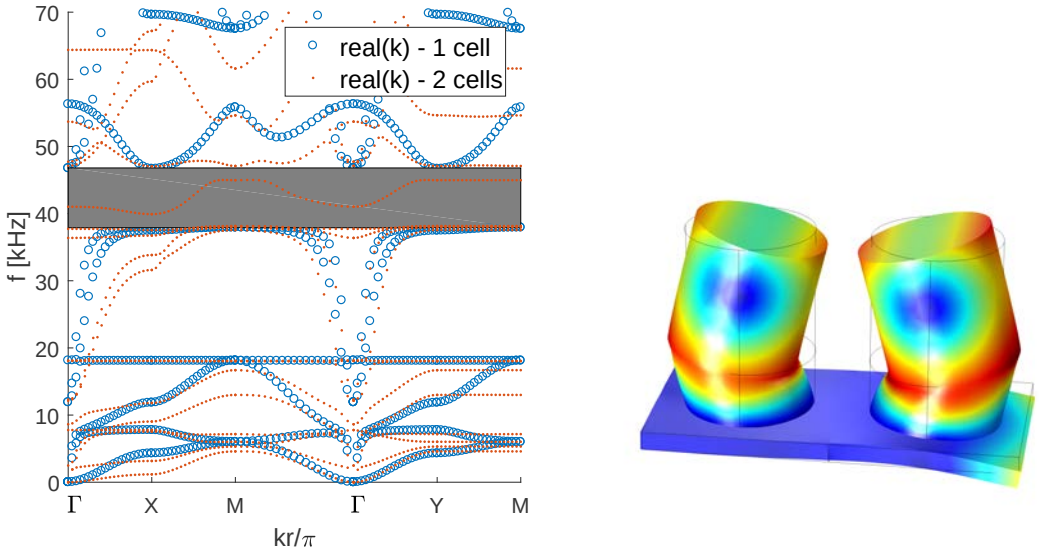

(a) (b)

Figure 11. a) Dispersion curves along the Brillouin zone obtained with the "Shifted-cell operator" method for the 1 cell and 2 cells system. b) Deformed shape at 41 kHz.

5. CONCLUSION

In this article, a metamaterial mixing aluminum with a dissipative polymer interface is designed. A 3D finite element model of the metamaterial elementary cell is designed for dispersion analysis using the "Shifted-cell operator" method. In order to validate the design of the metamaterial, a complete 3D model integrating an interface composed of a distributed set of unit cells is presented. The attenuation in finite structure is not as important as that predicted by the bandgap in infinite structure. Energy propagates along each edges of the periodic lattice. This point is confirmed through experimental measurements. Boundary conditions are really important in this case and the dispersion analysis can not predict this effect. Finally, an extension of the Bloch approach is proposed to handle finite system boundary conditions in order to identify situations where energy transfer may arise because of reflections on the border of the domain.

ACKNOWLEDGMENTS

This work was financed by The French National Research Agency under grant number ANR-12-JS09-008-COVIA. It has been performed in cooperation with the Labex ACTION program (ANR-11-LABX-0001-01).

REFERENCES

[1] L. Brillouin, *Wave propagation in periodic structures*, Dover Publication, 1953.

[2] M. Hussein, M. Leamy, and M. Ruzzene, "Dynamics of phononic materials and structures: Historical origins, recent progress, and future outlook," *Applied Mechanics Reviews* **66**(4), p. 040802, 2014.

[3] S. Shan, S. Kang, Z. Zhao, L. Fang, and K. Bertoldi, "Design of planar isotropic negative poissons ratio structures," *Extreme Mechanics Letters* **4**, pp. 96–102, 2015.

[4] A. Slann, W. White, F. Scarpa, K. Boba, and I. Farrow, "Cellular plates with auxetic rectangular perforations," *physica status solidi (b)* **252**(7), pp. 1533–1539, 2015.

[5] K. Billon, I. Zampetakis, F. Scarpa, M. Ouisse, E. Sadoulet-Reboul, M. Collet, A. Perriman, and A. Hetherington, "Mechanics and band gaps in hierarchical auxetic rectangular perforated composite metamaterials," *Composite Structures* **160**, pp. 1042–1050, 2017.

[6] J. Joannopoulos, S. Johnson, J. Winn, and R. Meade, *Photonic crystals: molding the flow of light*, Princeton university press, 2011.

[7] G. Floquet, "Sur les équations différentielles linéaires à coefficients périodiques," in *Annales scientifiques de l'École normale supérieure*, **12**, pp. 47–88, 1883.

[8] F. Bloch, "Über die quantenmechanik der elektronen in kristallgittern," *Zeitschrift für physik* **52**(7-8), pp. 555–600, 1929.

[9] M. Collet, M. Ouisse, M. Ruzzene, and M. Ichchou, "Floquet–bloch decomposition for the computation of dispersion of two-dimensional periodic, damped mechanical systems," *International Journal of Solids and Structures* **48**(20), pp. 2837–2848, 2011.

[10] K. Billon, M. Ouisse, E. Sadoulet-Reboul, and M. Collet, "Numerical tools for efficient simulations of wave propagation in damped periodic structures," in *INTER-NOISE and NOISE-CON Congress and Conference Proceedings*, **251**(1), pp. 889–896, Institute of Noise Control Engineering, 2015.

[11] T. Wu, T. Wu, and J. Hsu, "Waveguiding and frequency selection of lamb waves in a plate with a periodic stubbed surface," *Physical Review B* **79**(10), p. 104306, 2009.

[12] K. Billon, M. Ouisse, E. Sadoulet-Reboul, M. Collet, and A. Khelif, "A two-state phononic crystal using highly dissipative polymeric material interface," 2015.

[13] K. Billon, M. Ouisse, E. Sadoulet-Reboul, M. Collet, G. Chevalier, and A. Khelif, "Design and experimental validation of an adaptive phononic crystal using highly dissipative polymeric material interface," in *SPIE Smart Structures and Materials+ Nondestructive Evaluation and Health Monitoring*, pp. 101640O–101640O, International Society for Optics and Photonics, 2017.

[14] P. Butaud, *Contribution à l'utilisation des polymères à mémoire de forme pour les structures à amortissement contrôlé*. PhD thesis, 2015.

[15] P. Butaud, E. Foltête, and M. Ouisse, "Sandwich structures with tunable damping properties: On the use of shape memory polymer as viscoelastic core," *Composite Structures* **153**, pp. 401–408, 2016.